Integrated Method for Boundary Delineation of Agricultural Fields in Multispectral Satellite Images

Anna Rydberg and Gunilla Borgefors, *Senior Member, IEEE*

***Abstract*—Most agricultural statistics are calculated per field, and it is well known that classification procedures for homogeneous objects produce better results than per-pixel classification. In this study, a multispectral segmentation method for automated delineation of agricultural field boundaries in remotely sensed images is presented. Edge information from a gradient edge detector is integrated with a segmentation algorithm. The multispectral edge detector uses all available multispectral information by adding the magnitudes and directions of edges derived from edge detection in single bands. The addition is weighted by edge direction, to remove "noise" and to enhance the major direction. The resulting edge from the edge detection algorithm is combined with a segmentation method based on a simple ISODATA algorithm, where the initial centroids are decided by the distances to the edges from the edge detection step. From this procedure, the number of regions will most likely exceed the actual number of fields in the image and merging of regions is performed. By calculating the mean and covariance matrix for pixels of neighboring regions, regions with a high generalized likelihood-ratio test quantity will be merged. In this way, information from several spectral bands (and/or different dates) can be used for delineating field borders with different characteristics. The introduction of the ISODATA classifier compared with a previously used region growing procedure improves the output. Some results are compared with manually extracted field boundaries.**

***Index Terms*—Edge detection, field boundaries, merging, segmentation.**

I. Introduction

AGRICULTURAL statistics are often obtained per field, which makes it essential to accurately define field boundaries of agricultural land parcels. Crop classification produces better results from a per-field classification than from a per-pixel classification, and it is desirable that pixels from field boundaries are excluded from the classification process. However, the within-field variance may sometimes be greater than the between-field variance, which complicates the decision making made from spectral observations. Both the within-field and the between-field variance of the spectral reflectance change with soil moisture or different crop phenological stages, depending on the time of acquisition during the growing season. Therefore, in order to detect field boundaries more accurately, image time series are often necessary.

An edge can be defined as a discontinuity in grey-level, color, texture, etc. [1], and can be both crisp and fuzzy. In our study, the edges we are interested in are the field boundaries of agricultural land parcels. Here, field boundaries are defined as boundaries where a change in crop type takes place or where two similar crops are separated by a natural disruption in the landscape, like a ditch or a road. A physically homogeneous field can, in other words, be divided into smaller parts, where the farmer is growing different crops in different parts of the field. This definition is chosen for the purpose of crop classification, where it is important to separate different crops from each other in a clustering procedure.

Normally, the natural boundaries, depending on imaging scale, constitute stronger spectral differences in an image than different crop types. Depending on the crop types and the phenological stage of the crop, these boundaries might not be spectrally separable at all or constitute a smooth transition rather than a sharp edge. This fact makes it important to find straight boundaries even though they may be weak. It is also important that time sequences of images are used in order to be able to separate different crops from each other. The within-field variance, on the other hand, is often greatest close to, and parallel to, a physical field boundary [2], which increases the risk of detecting false double field boundaries.

By integrating different methods of segmentation, the advantages of each method can be used, in combination with special care taken of the specific feature of interest, to improve the segmentation output for this specific feature.

In this study, an integrated method designed for multispectral and multitemporal image information is presented. Multispectral edge information from a gradient edge detector is integrated with segmentation achieved by a simple ISODATA classifier [3]. Each segment is then labeled to have its own identity number. From the segmentation procedure, the number of regions will exceed the actual number of fields in the image and a merging of regions is performed. By calculating the mean and covariance matrix for pixels of neighboring regions, the regions with a high generalized likelihood-ratio test quantity will be merged.

Combining edge detection and different segmentation procedures is not a new idea [4]–[9]. The combination of the two methods yields far better results than those of a single method. One approach is made by [10] which starts with a split-and-merge algorithm resulting in a deliberate oversegmentation of the image. The boundaries of the region are then eliminated or modified on the basis of criteria that integrate contrast with boundary smoothness, variation of the image gradient along the boundary, and a criterion that penalizes for the presence of artifacts reflecting the data structure used during segmentation (quad-tree in this case). A variant of this technique is presented

Manuscript received September 29, 2000; revised August 29, 2001.

The authors are with the Centre for Image Analysis, Swedish University of Agricultural Sciences (SLU), Uppsala, Sweden (e-mail: anna.rydberg@cb.slu.se).

Publisher Item Identifier S 0196-2892(01)10406-7.

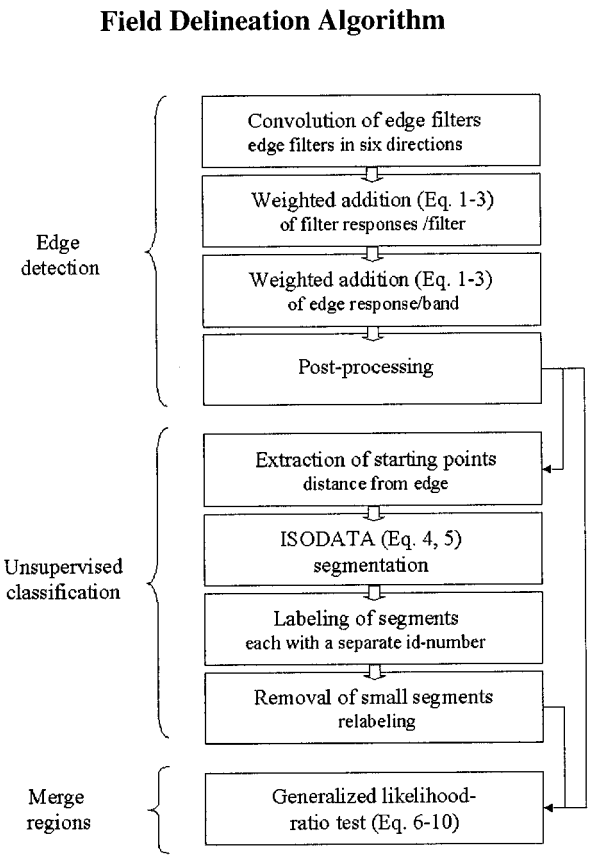

Fig. 1. Flowchart of the segmentation algorithm for agricultural fields.

in [11]. However, performance can be improved by combining edge detectors with segmentation procedures that both utilize information from multiple band sources.

Methods integrating image information with map information are presented in [12] and [13], where accuracy of segmentation and subsequent classification are shown to be superior to traditional automatic techniques. In our study, however, map information is not taken into consideration.

II. Method

The algorithm for delineating agricultural field boundaries is divided into three parts. The first part is a multispectral edge detection where the main boundaries are found and correctly located. The second step is an unsupervised classification using an ISODATA algorithm [3] integrated with the results from the edge detection step and the third step is to merge regions from the over-segmentation in step two. Fig. 1 shows the flow diagram of the main processing steps of the field delineation algorithm.

An area of Southern Sweden in the county of Västra Götaland, Sweden, will be used as an example site. In Fig. 2, the near infrared band from a SPOT satellite image of part of the study area is shown. A manual segmentation was made over the same area to serve as ground truth. Areas of forests and other land not used as farmland are not of interest and are therefore not manually segmented (black zones). Results will also be exemplified for TM data.

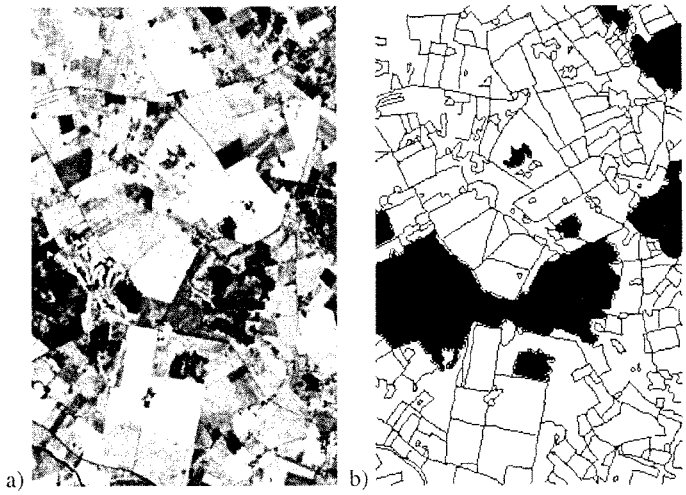

Fig. 2. (a) Near infrared SPOT image (band 3) over the study site. (b) Manually segmented image (ground truth).

A. Edge Detection

The multispectral edge detector used in this integrated method for boundary delineation is a gradient-based method, where both magnitude and direction of the edges are calculated [14]. This edge detector, based on the Nevatia-Babu linear edge detector [15] determines the edge magnitude and direction in an image by convolution with six 5×5 edge filters, each representing an angle between 0° and 150°. The outputs of all six filters are added vector-wise, using computed magnitudes and fixed filter directions. Since the filter responses are represented in discrete 30° intervals, a more correct direction is achieved if not only the max-vector is considered, which is the case in the Nevatia-Babu edge detector, since the correct direction of the gradient may be between two filter directions, see Fig. 4. The vectors are weighted prior to addition in order to remove noise and enhance the accuracy of the true vector direction, see (1)–(3) in the following.

The method for weighted vector addition [14] uses the responses from single masks $\bar{v}_i$, which are added to a vector sum $\bar{v}_{\text{tot}}$ as follows:

$$\bar{v}_{\text{tot}} = \sum_{i=1}^{n} w_i \bar{v}_i \quad \text{where} \tag{1}$$

$$w_i = (\cos \Theta_i)^{\alpha}, \quad \text{and} \tag{2}$$

$$\Theta_i = \arg(\max(\bar{v}_{1-n})) - \arg(\bar{v}_i) \tag{3}$$

where w_i is the weight for every vector $\bar{v}_i$, and n is the total number of vectors to be added. The weights are calculated by taking the cosine of Θ, which is the difference between the angle of the investigated vector and the largest vector. The result is raised to α, which decides the degree of weight. Here, at the filter addition step, α is set to 1 to make the weighting effect small.

Addition of vectors in the directions between 0° and 180° can be made in numerous ways, with completely different vectors as a result. Using the simple vector sum gradient will attenuate edges for nearly opposite gradient components. This is not desirable. What is really wanted is attenuating responses

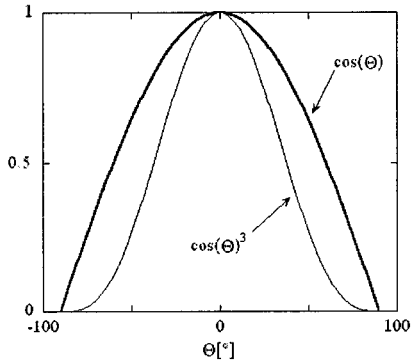

Fig. 3. Filter responses and edge responses from different channels are weighted slightly differently (α) before vector addition using the weighted function in the diagram.

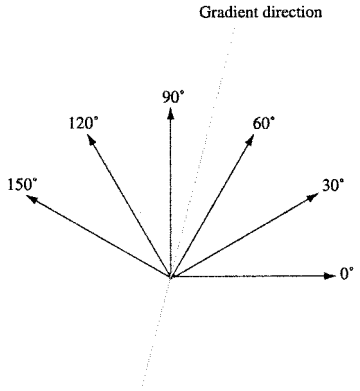

Fig. 4. Filter responses are generated from one single image, but the correct direction of the gradient can be located between two filter responses.

differing 90° (see discussion adding responses from different bands). This is the case if the vector sum is calculated using the double angle, i.e., the direction is given by doubling the angle of the filter direction. By adding the vector components in this way, the vector sum is both computationally cheap and accurate. Due to the double angle procedure, $\bar{v}_{\mathrm{tot}}$ in (1) has to be divided by two to represent the correct angle.

When a single edge image has been derived for each spectral band, this edge information is added in a similar way, but with n vectors from n input image bands. Since the direction of the same edge in different wavelength bands, due to different transitions from dark to bright areas in different wavelengths, may be in opposite directions, all edge directions are converted to the interval 0° to 180°.

Here, α is set to three to enhance the weighting effect, since agricultural fields seldom have corners with small acute angles. In this way, edges with a lower magnitude, which are present in all spectral bands, are identified at the same time as noise is attenuated, since noise does not have the same distinct direction in all images. These advantages disappear if, instead, the maximum edge strength in any of the bands is used.

Fig. 3 illustrates the functions used for weighting where the max-vector ($\Theta_i = 0$) has the biggest influence on the output vector and the vector perpendicular to the max-vector has no influence at all.

For the edge vector addition from the different spectral bands, the different bands may actually contain information

Fig. 5. Resulting edges from the edge detection step.

from different edges. However, weak edges with the same direction present in all bands should be considered as a rather strong edge. This can be achieved if all edge information is taken into consideration and not only the maximum. In the case of a corner, for instance, or the crossing of a strong edge by a weaker one, it is important that the edge response is weakened since it is not really an edge, or that the the weaker edge is even more suppressed.

The resulting edge image is then thinned using magnitude and direction information, together with hysteresis thresholding [16], so that edges with a lower magnitude can be preserved without adding a significant amount of noise. Then small gaps in the edge segments are filled in. For details, see [14]. Results of edge detection are found in Fig. 5.

This edge detection algorithm does not result in closed contours. In fact, where two perpendicular edges intersect, the intersecting pixels are removed in the thinning step. Generally, gradient-based filtering generates edges with smoothed corners and intersections, especially if the filter size is larger than 3×3. The thinning procedure is purposely designed to remove these parts as the aim of this study is to detect field boundaries, which are known to usually have sharp corners. Instead, these discontinuities, and larger gaps where the method failed to detect edges, must be closed by postprocessing or by using additional procedures, such as some kind of segmentation.

B. Unsupervised Classification Using ISODATA

The resulting edges from the multispectral edge detection algorithm are combined with a segmentation method based on an unsupervised ISODATA classifier. The original ISODATA classifier [17] assigns each pixel to a candidate cluster created by calculating mean vectors, where each pixel is represented by a vector of spectral values, and using $+/-$ one standard deviation in all spectral bands. Each pixel is compared with each cluster mean and assigned to the cluster where mean value is closest in the feature space using Euclidean distance. New mean values are calculated for the clusters, and the pixels are tested again against the new mean values. The procedure continues until the user-defined parameters, maximum number of iterations, and

Fig. 6. Distance map from the edges.

Fig. 7. Oversegmentation from the unsupervised classification step. Segmentation identities are marked by grey level.

little change in class assignment, are reached. All in all, six user-defined parameters must be specified.

The unsupervised classification method used in this paper is a simplified ISODATA algorithm [3], where only three, instead of six, user-specified variables control the clustering process. These are

- starting number of centroids;
- error tolerance on the dislocation of centroids;
- error tolerance on the number of members in each class.

Each iteration recalculates mean values and reclassifies pixels with respect to the new means to minimize the global distortion D (4). In our case, the new center point is simply the mass center of the cluster

$$D = D(k, \{c_i\}, \{C_i\}) = \mathbf{S}_{j=1\ldots n} \min_i (||x_j - c_i||^2). \quad (4)$$

The algorithm calculates class means $c_1, \ldots c_k$ from k number of centroids in a set $S = x_{j=1\ldots n}$ in the Euclidean space R^N and then iteratively assigns pixels x_j to the closest centroid $C(c_i)$ for each $C_i, i = 1 \ldots k$ using minimum distance techniques where the Euclidean distance in R^N is minimized (5). The clusters are denoted $C_1, \ldots, C_k$

$$||x - c_i||^2 = \min_{1 \le q \le n} (||x - c_q||^2) = \min_{1 \le q \le n} \mathbf{S}_{p=1\ldots N} (x_p - c_{q,p})^2. \quad (5)$$

This process continues until the number of pixels in each class changes by less than a selected pixel change threshold, depending on the spectral characteristics in the image. The parameters used here are deliberately set to oversegment the image.

Two input images are used in the classification step, the original image and the image from the edge detection step. Seedpoints, used as initial centroids in the ISODATA algorithm can be randomly chosen, but we prefer to place them in the centers of the biggest fields. The reason is that agricultural fields have greatest variance of crop growth close to the field boundaries and it is therefore important to avoid using initial points with spectral characteristics from such areas. The edge image is converted to a distance transform [18], where each pixel is given the value of the distance to the nearest edge, Fig. 6. The pixels that are furthest from any edges are used as seed points, as they have a large likelihood of being in the centers of large fields.

After the initial classification, small segments, i.e., segments containing four pixels, at the most, and completely surrounded by another region, are merged into the surrounding region.

If a pixel is an edge in the edge image, but belongs to a region after the classification step, this region is split into two regions divided by an edge. Finally, all segments are labeled to have their own unique identity number. Results are shown for the study site in Fig. 7.

C. Merging of Regions

The unsupervised classification procedure produces too many regions in the initial clustering step. By calculating the mean and covariance matrix (6) for pixels of neighboring regions, regions having a high generalized likelihood ratio test quantity (7) will be merged.

Neighboring regions are assumed to be as two multivariate normal distributions with mean vectors μ_1 and μ_2 and covariance matrices $\hat{\Sigma}_1$ and $\hat{\Sigma}_2$ in an image with b number of bands

$$\hat{\Sigma} = \frac{\sum_{i=1}^{b} (x_i x_i^T) - n\mu\mu^T}{n}. \quad (6)$$

The hypothesis $H_0 : \mu_1 = \mu_2$ and $\hat{\Sigma}_1 = \hat{\Sigma}_2$ is tested with a likelihood-ratio (LR) test. The test quantity used is the LR-quota

$$\Lambda = \frac{\max_{\mu,\Sigma} L(\mu, \Sigma; x, y)}{\max_{\mu_1 \Sigma_1, \mu_2 \Sigma_2} L(\mu_1, \Sigma_1; x) L(\mu_2, \Sigma_2; y)} \quad (7)$$

where L is the likelihood function, that is, the density function seen as a function of the parameters. The hypothesis H_0 is rejected if Λ is small. The independent observations $x_1, x_2, \ldots, x_n$ and $y_1, y_2, \ldots, y_m$ have $N(\mu_1, \Sigma_1)$ and $N(\mu_2, \Sigma_2)$ distributions, respectively, and refer to the pixels in two different regions.

If the digital numbers (DN) for different pixels are independent (which is not true), (7) can be simplified to

$$\Lambda = \frac{|\hat{\Sigma}_1|^{n/2} |\hat{\Sigma}_2|^{m/2}}{|\hat{\Sigma}_{1,2}|^{(n+m)/2}} \quad (8)$$

where $\hat{\Sigma}_1$ and $\hat{\Sigma}_2$ are the covariance matrixes for regions 1 and 2, respectively, and m and n are the number of pixels in each region.The covariance matrix for the merged region is $\Sigma_{1,2}$, i.e., regions 1 and 2 together.

We calculate (9), and then neighboring regions are merged according to similarity in covariance matrices. Regions next to each other are merged in descending order. That is, region pairs resulting in the smallest value of λ are merged first.

$$\lambda = -n\log|\hat{\Sigma}_1| - m\log|\hat{\Sigma}_2| + (n+m)\log|\hat{\Sigma}_{1,2}|. \quad (9)$$

The merging of regions continues as long as the total average field size does not exceed the defined threshold (based on *a priori* knowledge from the study area) or until no changes occur. Equation (9) has a χ^2-distribution with df degrees of freedom according to (10), where p is the number of input bands used in the study

$$\mathrm{df} = p + \frac{p(p+1)}{2}. \quad (10)$$

A special case has to be considered if the determinant of the covariance matrix for a region is close to 0, i.e., if the region is very homogeneous. If so, the difference between all the spectral bands means between the two regions are considered. If it is smaller than the threshold used for the region growing procedure, then the regions are merged. In this way, information from several spectral bands (and/or different dates) can be used for delineating field boundaries with different characteristics.

Finally, to be able to compare edges and segments with ground truth data, all regions were represented with their boundaries as edges. This resulted in edges three pixels wide at some places, so therefore a simple thinning of the edges was performed to achieve the final output edges from the algorithm.

III. Results

Agricultural fields often have rather large variance in connection with field boundaries due to vehicle transition zones. At the same time, this is a problematic region in images as well, due to the occurrence of mixed pixels. Region growing procedures seems to fail to correctly segment such areas. In previous work [19] we used the region growing segmenter instead of the ISODATA. It gave significantly worse results. In Fig. 8, an example is presented of how region growing [19] tends to stop before the actual field boundary is reached. To solve this, the simplified ISODATA classifier is used in combination with multispectral edge detection.

The method presented in this paper was tested on different images and also compared with interpreted boundaries. Both Landsat TM and SPOT images were used, see Fig. 9.

Some of the output edges from the algorithm used in this study were compared to manually segmented edges over the same area. The manual segmentation was created from the same original multispectral SPOT image as the segmentation and was considered as ground truth (GT) in this study. The evaluation of the results was made by comparing the distances between edges in the two edge images using a weighted [Chamfer (3, 4)] distance transform [20], Fig. 6. To be able to detect differences for both oversegmented and missing edges, the distances were compared in both ways, i.e., each edge image was compared with the corresponding edge locations in the opposite edge distance image. Fig. 10 shows that the segmentation algorithm finds too many edges, with more than 13% of the detected edges having a distance greater than three pixels from a true edge. Some edges, however, still remain to be located, but 83% of the GT-edges are identified by the algorithm at correct pixels or at a distance of 1 from correct pixels.

The initial regions created by the classification step determine where the final boundary is to be located. The order in which regions are merged is very important for the outcome and in this study, the order seems to be appropriate.

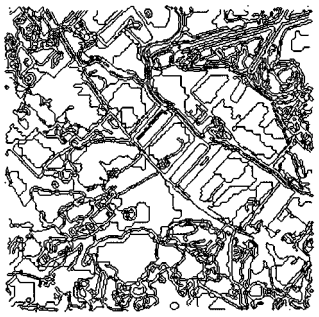

Fig. 8. Region growing alone tends to stop before field boundaries are reached.

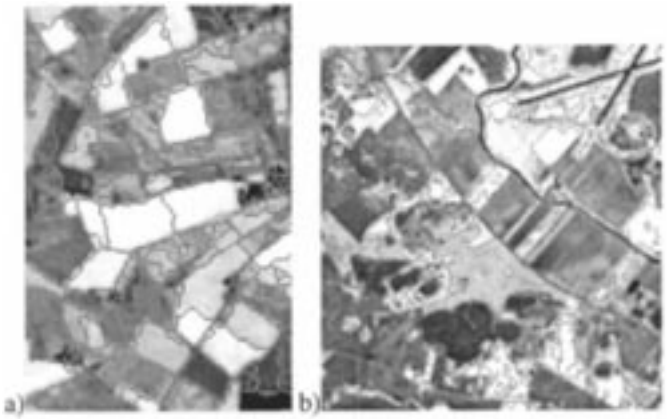

Fig. 9. (a) Landsat TM Image and (b) SPOT image overlaid by boundaries from the delineation algorithm.

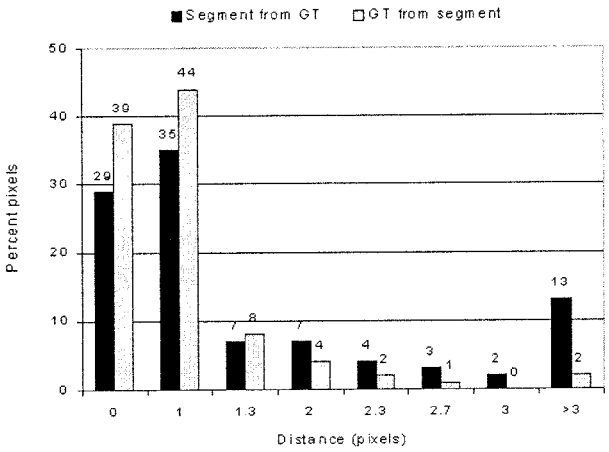

Fig. 10. Distances from the segmented edge image to ground truth and vice versa.

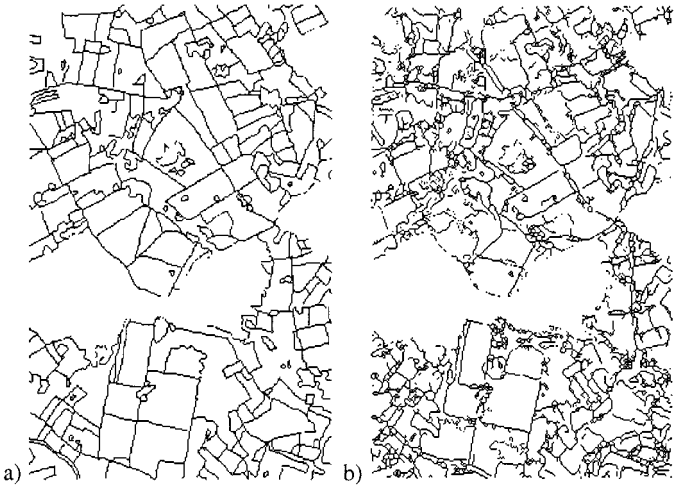

Fig. 11. (a) Manually segmented image and (b) image segmented by the delineation algorithm.

The final image resulting from this algorithm, see Fig. 11, needs further postprocessing, especially removal of short edges and closing of corners and gaps. Some further merging of too small areas may also be required if such *a priori* knowledge about field size is available. The result can then be vectorized for future integration in a GIS.

IV. Discussion and Conclusions

Different kinds of images have different spectral responses and spatial resolution that affect the overall variation in the image. For instance, the SPOT image has a higher spatial resolution than a Landsat TM image and contains more spatial variation between neighboring pixels. It therefore requires different thresholds at the classification step than the Landsat TM image.

When the human brain analyzes an image, numerous sophisticated segmentation procedures take place, many of which use texture information rather than spectral information. Nagao and Matsuama [21] have developed a system that is relatively insensitive to changes in solar illumination and atmospheric conditions. Emphasis is placed on geometric features such as size and shape, rather than on spectral features. Region features like texture, concavity, compactness, boundary straightness, and region size are calculated. These features can be useful when post-processing the results of our method. We have presented a method for field delineation in remotely sensed images. It uses information from all spectral bands both for finding edges and for clustering pixels into homogeneous areas. The method is completely automatic and unsupervised, but the operator needs to set some thresholds depending on the type of actual data. When compared with a manual delineation, the results are shown to be quite promising, with 87% of the GT-edges found and only about 13% of the edges found not corresponding to GT-edges. Some of these extra edges, in fact, correspond to visible within-field variations, so they cannot be called false.

A rule of thumb is to make decisions as late as possible in processing the image. Special care can also be taken in agricultural areas to account for the within-field variance.

Acknowledgment

The authors would like to thank the Swedish Farming Association (ODAL), Lidköping, Sweden, for images and Dr. E. Piazza for ISODATA program code.

References

[1] M. Sonka, V. Hlavac, and R. Boyle, *Image Processing, Analysis, and Machine Vision*, 2nd ed. Pacific Grove, CA: PWS, 1998.
[2] A. Rydberg and M. Söderström, "Relative potential crop growth assessment from remotely sensed images compared to ordinary yield maps," in *Proc. 5th Int. Conf. Precision Agriculture*, P. Robert, Ed., Minneapolis, MN, July 16–19, 2000.
[3] E. Piazza, "Comparison of different classification algorithms of NOAA AVHRR images," Proc. SPIE, July 2000.
[4] R. L. Ketting and D. A. Landgrebe, "Classification of multispectral image data by extraction and classification of homogenous object," *IEEE Trans. Geosci. Remote Sensing*, vol. GE-14, pp. 19–26, Jan. 1976.
[5] J. P. Gambotto, "A new approach to combining region growing and edge detection," *Pattern Recognit. Lett.*, vol. 14, pp. 869–875, Nov. 1993.
[6] J. H. Haddon and J. F. Boyce, "Co-occurrence matrices for image analysis," *Electron. Commun. Eng. J.*, vol. 5, no. 2, pp. 71–83, 1993.
[7] J. Le Moigne and J. C. Tilton, "Refining image segmentation by integration of edge and region, data," *IEEE Trans. Geosci. Remote Sensing*, vol. 33, pp. 605–615, May 1995.
[8] R. P. H. M. Schoenmakers, "Integrated Methodology for Segmentation of Large Optical Satellite Images in Land Applications of Remote Sensing," Katholieke Univ., Nijmegen, The Netherlands, Sept. 13, 1995.
[9] A. Lopès, R. Fjørtoft, D. Ducrot, P. Marthon, and C. Lemaechal, "Edge detection and segmentation of SAR images in homogeneous regions," in *Information Processing for Remote Sensing*, C. H. Chen, Ed., Singapore, World Scientific, 1999.
[10] T. Pavlidis and Y. T. Liow, "Integrating region growing and edge detection," *IEEE Trans. Pattern Anal. Maching Intell.*, vol. 12, pp. 225–233, Mar. 1990.
[11] J. Garcia-Consuega and A. Martìnez, "ECep-echo: Extraction and classification of edge pixels in an echo approach," in *Remote Sensing in the 21st Century: Economic and Environmental Applications*, J. L. Casanova, Ed. Rotterdam, The Netherlands: A. A. Balkema, 2000, pp. 261–266.
[12] D. G. Corr, A. M. Tailor, A. Cross, D. C. Hoggs, D. H. Lawrence, D. C. Mason, and M. Petrou, "Progress in automatic analysis of multitemporal remotely-sensed data," *Int. J. Remote Sensing*, vol. 10, pp. 1175–1195, 1989.
[13] D. C. Mason, D. G. Corr, A. Cross, D. C. Hoggs, M. Petrou, D. H. Lawrence, and A. M. Tailor, "The use of digital map data in the segmentation and classification of remotely-sensed iamges," *Int. J. Geograph. Inform. Syst.*, vol. 2, pp. 195–215, 1988.
[14] A. Rydberg and G. Borgefors, "Extracting multispectral edges in satellite images over argicultural fields," in *10th Int. Conf. Image Analysis and Processing*, Venice, Italy, Sept. 27–29, 1999, pp. 786–791.
[15] R. Nevatia and K. R. Babu, "Linear feature extraction and desscription," *Comput. Graph. Image Processing*, vol. 13, pp. 257–269, 1980.
[16] J. Canny, "A computational approach to edge detection," *IEEE Trans. Pattern Anal. Machine Intell.*, vol. PAMI-8, pp. 679–698, Nov. 1986.
[17] D. Hall and G. Ball, Isodata: A Novel Method of Data Analysis and Pattern Classification, 1965.
[18] G. Borgefors, "Distance transforms in digital images," *Comput. Vis. Graph. Image Processing*, vol. 34, pp. 344–371, 1986.
[19] A. Rydberg, "Integrated method for boundary delineation of agricultural fields in multispectral satellite image," in *Proc. IGARSS'00*, Honolulu, HI, July 23–28, 2000, pp. 1678–1680.
[20] G. Borgefors, "Hierarchial chamfer matching: A paramertic edge matching algorithm," *IEEE Trans. Pattern Anal. Machine Intell.*, vol. 6, pp. 849–865, Nov. 1988.
[21] M. Nagao and T. Matsuyama, *A Structural Analysis of Complex Aerial Photographs*. New York: Plenum, 1980.

Anna Rydberg was awarded the M.Sc. degree in physical geography from Uppsala University, Uppsala, Sweden, in 1995. She is currently pursuing the Ph.D. degree at the Centre for Image Analysis, Swedish University of Agricultural Sciences, Uppsala, Sweden.

Her present research interest in image analysis is automated segmentation of agricultural field boundaries in remotely sensed images.

Gunilla Borgefors (SM'98) received the M.Eng., Lic.Eng. degrees in applied mathematics and the "Docent" degree in image processing from Linköping University, Linköping, Sweden, in 1975, 1983, and 1992, respectively, and the Ph.D. degree in numerical analysis from the Royal Institute of Technology, Stockholm, Sweden, in 1986.

From 1982 to 1993, she was employed at the National Defence Research Establishment, Linköping, Sweden, becoming Director of Research for computer vision, and from 1990 to 1993, she was Head of the Division of Information Systems. Since 1993, she has been a full Professor at the Centre for Image Analysis, Swedish University of Agricultural Sciences and Uppsala University, Sweden, and since 1996, she has been Head of the same center. She has published a large number of papers in international journals and conferences, and has been the editor of four books on image analysis. Her current research interests are digital geometry in two, three, and higher dimensions, data fusion, and the use of image analysis in remote sensing, forestry, and many other applications. More data can be found at http://www.cb.uu.se/gunilla/.

Dr. Borgefors is a member of the Royal Society of Sciences in Uppsala and a Fellow of International Association for Pattern Recognition. She was President of the Swedish Society for Automated Image Analysis from 1988 to 1992, and Secretary and First Vice President of the International Association for Pattern Recognition from 1990 to 1994 and 1994 to 1996, respectively.